Available online at www.sciencedirect.com
ScienceDirect
Journal of Catalysis 243 (2006) 350–359
JOURNAL OF CATALYSIS
www.elsevier.com/locate/jcat

A study of propane ammoxidation on Mo–V–Nb–Te-oxide catalysts diluted with Al_2O_3, SiO_2, and TiO_2

Johan Holmberg, Robert Häggblad, Arne Andersson *

Department of Chemical Engineering, Lund University, Center for Chemistry & Chemical Engineering, P.O. Box 124, SE-221 00 Lund, Sweden

Received 8 June 2006; revised 31 July 2006; accepted 15 August 2006

Available online 15 September 2006

Abstract

Mo–V–Nb–Te-oxide catalysts with nominal metal compositions equal to those of M1, M2, and a mixture of the M1 and M2 phases were prepared in neat and sol-diluted forms. The latter catalysts were prepared with 30 wt% of Al_2O_3, SiO_2, or TiO_2 sol. All catalysts were characterized by BET, XRD, and TPR and tested for the respective ammoxidation of propane and propene. XRD showed that dilution with SiO_2 gave catalysts with the pure M1 and M2 phases. Al_2O_3 was found to react with Mo and V, giving catalysts with $Al_2(MoO_4)_3$, $AlVO_4$, $TeMo_5O_{16}$, Nb_2O_5, and, in one case, M2. Dilution of the nominal M1 composition with TiO_2 produced $Mo_{5-x}(V/Nb/Te)_xO_{14}$, whereas the M2 and M1/M2 nominal compositions gave the correct type of phases. TPR and XRD reveal that dilution with SiO_2 gives improved dispersion of M1 and M2; however, the dilution effect is greater, resulting in no improved activity when expressed per unit surface area of the catalyst. For propane ammoxidation, the activity data show that the neat M1 and M1/M2 catalysts are the best samples. The corresponding SiO_2-diluted catalysts are less active and selective. For the ammoxidation of propene, the neat M1 and the SiO_2-diluted M1 are the two best catalysts in terms of both activity and selectivity. More selective catalysts with lower activity and some acrolein formation are the neat M2 phase and M2 diluted with TiO_2 or SiO_2.

Keywords: Ammoxidation; Propane; Propene; Acrylonitrile; Mo–V–Nb–Te–O_x catalysts; Al_2O_3; SiO_2; TiO_2; BET; XRD; TPR

1. Introduction

In the field of catalysis, many not-yet commercialized processes are interesting from an economical standpoint. However, many of these processes are still waiting a technological breakthrough to improve yields before they can be used on an industrial scale. The ammoxidation of propane to produce acrylonitrile is such a process. Considering the annual market for acrylonitrile of 5500 ktons, the intense interest in the development of competitive catalyst systems for propane ammoxidation is understandable [1]. The most promising system so far is the Mo–V–Nb–Te-oxide system, originating from the Mo_5O_{14} system [2,3]. The primary patents, reporting yields up to 62% of acrylonitrile, are held by Mitsubishi [4] and Asahi [5].

Several studies have been performed on the catalytic performance and the crystal structures of the Mo–V–Nb–Te–O system. The system comprises two orthorhombic phases, termed M1 and M2 (pseudo-hexagonal) [6,7], with the respective general compositions $(TeO)_{2-2x}(Te_2O)_xM_{20}O_{56}$ ($0 \leqslant x \leqslant 1$, M = Mo, V and Nb) and $(TeO)_2M_6O_{18}$ (M = Mo, V, either with or without Nb) [8,9]. The structures of M1 and M2 are related to those of $Cs_{0.7}(Nb_{2.7}W_{2.3})O_{14}$ [10] and KW_3O_9 [11], respectively. In both M1 and M2, the Te atoms occupy hexagonal channels, consistent with the alkali analogues having the alkali metal in similar coordination. Because the hexagonal channels in M1 and M2 do not have to be completely filled with Te–O units [7], and due to the related multivalency of the structures, it follows that the Te content of M1 and M2 can vary.

Previously published results have shown that the conversion of propane to acrylonitrile occurs via intermediate propene, with the M1 phase alone being the paraffin-activating phase [12,13]. Other studies have indicated that bulk M2, in contrast to bulk M1, does not contain pentavalent vanadium [7,14], which is the generally accepted explanation for the finding that M2 is unable to activate propane [15]. Both phases do contain Mo and Te, which are believed to be active for the consecutive

* Corresponding author.
E-mail address: arne.andersson@chemeng.lth.se (A. Andersson).

0021-9517/$ – see front matter
doi:10.1016/j.jcat.2006.08.008

transformation of formed propene to acrylonitrile. Even though the M1 phase can single-handedly convert propane to acrylonitrile, earlier studies have shown that the best catalysts consist of both phases [13,15]. Because the M2 phase is more selective than M1 for the conversion of propene to acrylonitrile [13], it is desirable to create a synergy between the phases where the M1 phase converts propane to propene, which then reacts on M2 to form acrylonitrile. To accomplish this symbiosis, the phases must be well mixed, preferably on the nanoscale [13].

Several options are available for improving the catalyst system. One possibility is to improve the performance of the respective M1 and M2 phase by tuning, through either substitution or adding promoters. Recently, we showed that it is possible to increase both the activity and the selectivity of the M2 phase by replacing Mo and V with W and Ti, respectively [16]. An alternative approach is to improve the interplay (i.e., the synergy between the two phases) by increasing the dispersion of the active material. Regarding to the latter objective, in this paper we explore the use of Al_2O_3, SiO_2, and TiO_2 sols as additives to M1, M2, and M1/M2 for use in the ammoxidation of propane and propene. Moreover, sol dilution of the catalyst is of interest for use in fluid-bed applications to increase the attrition resistance of the catalyst and to reduce the production cost of the catalyst.

2. Experimental

2.1. Catalyst preparation

Catalysts were prepared with synthesis compositions of the active metals corresponding to $Mo_1V_{0.20}Nb_{0.13}Te_{0.11}$, $Mo_1V_{0.5}Te_{0.5}$, and $Mo_1V_{0.33}Nb_{0.11}Te_{0.22}$, which are denoted X1, X2, and X3, respectively. For each composition, both neat (undiluted) and sol-diluted catalysts were prepared. Neat catalysts were prepared using the precursor method. The desired amounts of $(NH_4)_6Mo_7O_{24}{\cdot}4H_2O$ (Merck), NH_4VO_3 (Kebo), and H_6TeO_6 (Fluka) were dissolved in water at 60 °C. When applicable, $Nb_2O_5{\cdot}5.5H_2O$ (Niobium Products Company) and $H_2C_2O_4{\cdot}2H_2O$ (Merck) were dissolved in a second water solution held at 60 °C (oxalic acid/Nb molar ratio = 2.75). For the preparation of the X1 and X3 catalysts, the two solutions were mixed for a short period, and the resulting mixture was dried rapidly as a 1-mm-thick layer on a hot pan held at 200 °C. Neat X2 compositions were prepared from the first solution only. In this case, after the desired amounts of the salts were dissolved in water at 60 °C, the water was evaporated under air at 150 °C overnight. All precursors were calcined in two steps, first under air at 275 °C for 2 h and then for another 2 h in a quartz reactor under a flow of argon at either 550 °C (X2) or 600 °C (X1 and X3).

The sol-diluted catalysts were prepared by adding Al_2O_3 (Nyacol AL20), SiO_2 (Grace Davison AS-40), or TiO_2 (Rhône-Poulenc) sol to the solution containing Mo, V, and Te. Apart from the addition of the sol, the catalysts were prepared following the same procedures as described above for the neat catalysts. The content of sol in the final product was 30 wt%.

Table 1
Notation, metal composition, sol additive and specific surface area of prepared samples

Catalyst notation	Active metal composition (metal ratios)	Sol	Specific surface area (m^2/g)
X1	$Mo_1V_{0.20}Nb_{0.13}Te_{0.11}$	–	6.1
X2	$Mo_1V_{0.5}Te_{0.5}$	–	2.5
X3	$Mo_1V_{0.33}Nb_{0.11}Te_{0.22}$	–	5.2
X1AS	$Mo_1V_{0.20}Nb_{0.13}Te_{0.11}$	Al_2O_3	16.8
X1SS	$Mo_1V_{0.20}Nb_{0.13}Te_{0.11}$	SiO_2	8.7
X1TS	$Mo_1V_{0.20}Nb_{0.13}Te_{0.11}$	TiO_2	1.3
X2AS	$Mo_1V_{0.5}Te_{0.5}$	Al_2O_3	7.6
X2SS	$Mo_1V_{0.5}Te_{0.5}$	SiO_2	6.5
X2TS	$Mo_1V_{0.5}Te_{0.5}$	TiO_2	4.7
X3AS	$Mo_1V_{0.33}Nb_{0.11}Te_{0.22}$	Al_2O_3	10.3
X3SS	$Mo_1V_{0.33}Nb_{0.11}Te_{0.22}$	SiO_2	7.7
X3TS	$Mo_1V_{0.33}Nb_{0.11}Te_{0.22}$	TiO_2	2.4

All samples were sieved, and the fraction of particles with diameters in the range of 250–425 μm was used for catalyst testing. The catalysts prepared, their notations, and specific surface areas are summarized in Table 1.

2.2. Activity measurements

The prepared catalysts were tested for the ammoxidation of propane and propene at atmospheric pressure and isothermal conditions using a stainless steel plug-flow microreactor. To improve the temperature control in the reaction zone, the reactor was embedded in an aluminium block and placed in a tube furnace. The feed composition was 6 vol% propane or propene, 7 vol% ammonia, 18 vol% oxygen, and 69 vol% argon. Catalytic data were collected at 400 °C for different space velocities by varying the catalyst load and/or the total flow rate, giving selectivity variations with the degree of conversion and allowing calculation of the activity. The catalyst loads varied from 0.02 to 2 g; loads <0.1 g were diluted 10 times by quartz particles of the same size as the catalyst. The total flow rate varied between 8.0 and 23.1 Ncm^3/min. Propane, propene, acrylonitrile, acetonitrile, acrolein, and CO_2 were analyzed on-line using a gas chromatograph equipped with a flame ionization detector, a thermal conductivity detector, and a Haysep Q column. CO was analyzed on-line with an IR instrument (Rosemount Binos 100). To avoid polymerization of the products, the exit line from the reactor to the gas chromatograph was kept at 200 °C.

2.3. Characterization

All fresh catalysts were examined by X-ray powder diffraction (XRD) on a Seifert 3000 TT diffractometer using Ni-filtered CuK_α radiation. The measurements were performed on ground samples using a rotating sample holder. Phase identification was made by comparison with JCPDS data files [17].

The specific surface areas of the catalysts were measured with a Micromeritics Flowsorb 2300 instrument. The single-point BET method was used with adsorption of nitrogen at liquid nitrogen temperature and subsequent desorption at room temperature. All samples were degassed at 200 °C for 24 h.

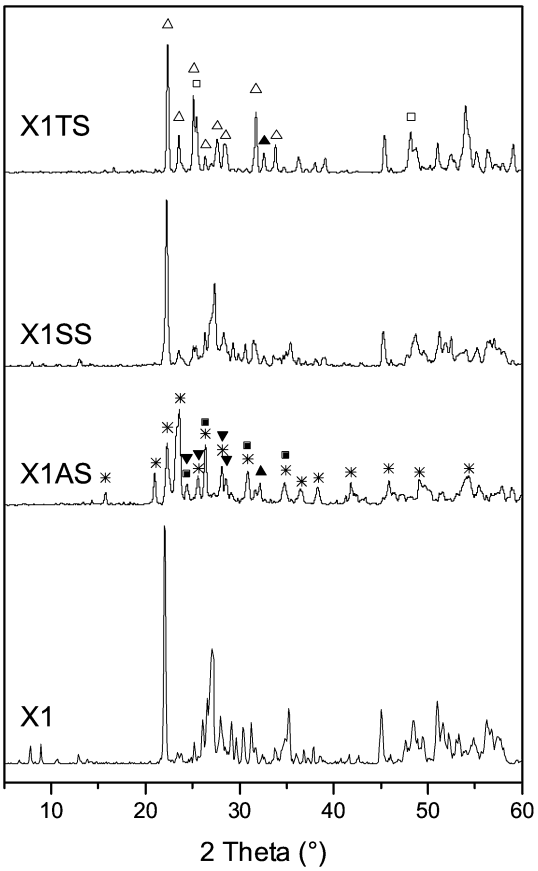

Fig. 1. X-ray diffraction patterns of the X1, X1AS, X1SS, and X1TS catalysts. Diffraction peaks not belonging to the M1 phase are marked as follows: $Al_2(MoO_4)_3$ (⁎), $AlVO_4$ (▼), $TeMo_5O_{16}$ (■), Nb_2O_5 (▲), $Mo_{5-x}(V/Nb)_xO_{14}$ (△), and TiO_2 (□).

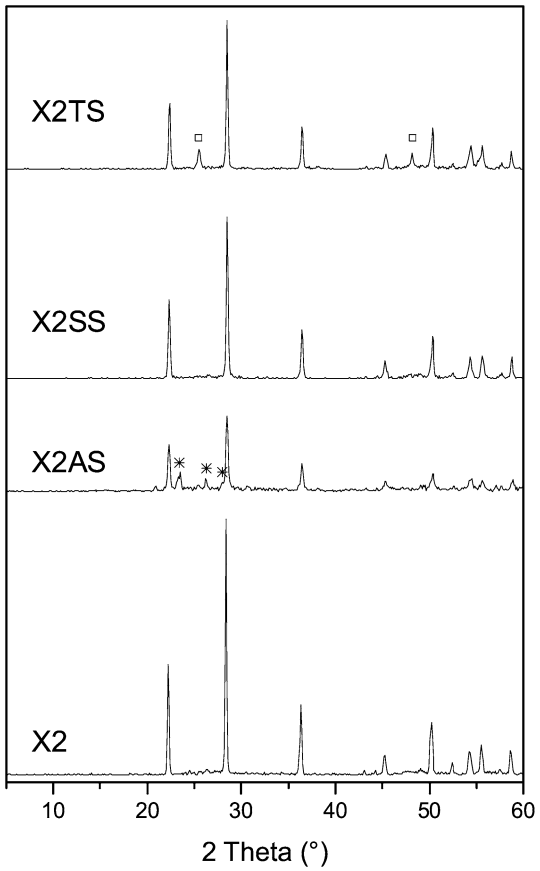

Fig. 2. X-ray diffraction patterns of the X2, X2AS, X2SS, and X2TS catalysts. Diffraction peaks not belonging to the M2 phase are marked as follows: $Al_2(MoO_4)_3$ (⁎) and TiO_2 (□).

Temperature-programmed reduction (TPR) was performed on a Micromeritics TPD/TPR 2900 instrument. The temperature was increased from 40 to 1000 °C at a rate of 10 °C/min. The reducing gas was 8.5 vol% H_2 in Ar, and a flow rate of 40 ml/min was used for a sample size of about 20 mg.

3. Results and discussion

3.1. X-ray diffraction

The diffraction patterns of the neat and the sol-diluted catalysts are displayed in Figs. 1–3. Comparing the four X1 catalysts (Fig. 1), the neat catalyst and the catalyst prepared with SiO_2 sol display only the diffraction peaks belonging to the M1 phase [7–9]. The sample prepared with Al_2O_3 sol, on the other hand, displays no peaks from M1 but does display peaks from $Al_2(MoO_4)_3$ (JCPDS 23-764) [17,18], $AlVO_4$ (JCPDS 31-34), $TeMo_5O_{16}$ (JCPDS 31-874), and Nb_2O_5 (JCPDS 32-710) [17]. In addition, the catalyst with TiO_2 additive shows no peaks from M1. In this case, the final catalyst gives mainly XRD lines from $Mo_{5-x}(V/Nb)_xO_{14}$ (JCPDS 31-1437 and 27-1310), Nb_2O_5, and the anatase polymorph of TiO_2 (JCPDS 21-1272) [17]. No diffraction peaks from any Te-containing phase are visible, which can be explained by the comparatively low Te content in the sample. Another possibility is that the V- and Nb-substituted Mo_5O_{14} structure [19] may contain some Te^{6+} as well, considering that 6-coordinated Te^{6+} and Mo^{6+} have similar ionic radii (0.70 and 0.73 Å, respectively) [20]. Moreover, loss of Te during the final heat treatment of the precursor in inert gas at 600 °C can occur if the intermediate calcination in air is performed at too low a temperature (∼150 °C) [12]. In the present study, however, the intermediate calcination was performed at higher temperature (275 °C), which is known to largely stabilize the Te in the precursor and give a product with a Te content roughly in agreement with starting composition of the synthesis [13].

Of the four X2 samples (Fig. 2), all four samples show diffraction peaks belonging to the M2 structure [7–9]. Moreover, the samples with Ti and Al display additional lines from TiO_2 (anatase) and $Al_2(MoO_4)_3$, respectively. Concerning the X3 catalysts (Fig. 3), the neat catalyst and the sample with SiO_2 both exhibit lines from the M1 and M2 phases exclusively, and the sample with Ti display some additional lines from TiO_2 (anatase). The sample with Al shows the same peaks as the X1AS catalyst, namely peaks from $Al_2(MoO_4)_3$, $AlVO_4$, $TeMo_5O_{16}$, and Nb_2O_5.

The phases identified in the samples by XRD are given in Table 2, showing that silica is the most inert additive with respect to the formations of M1 and M2. Alumina is the least inert of the additives, because it reacts with both Mo and V.

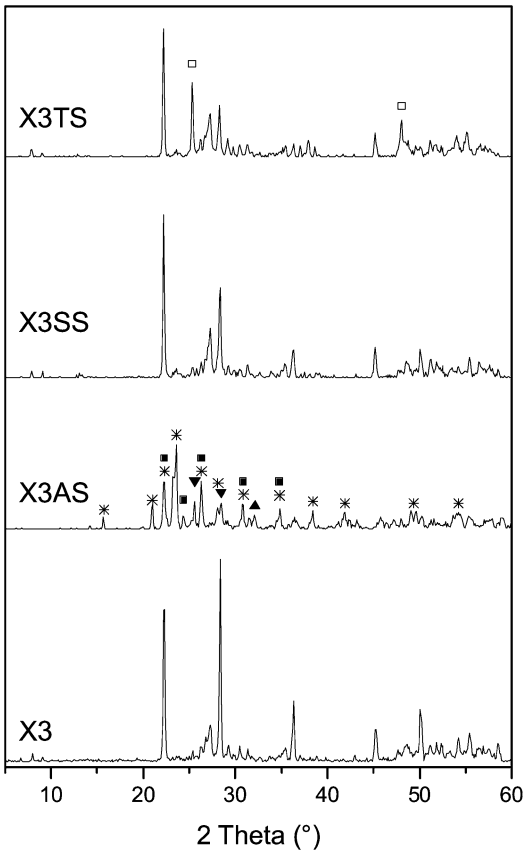

Fig. 3. X-ray diffraction patterns of the X3, X3AS, X3SS, and X3TS catalysts. Diffraction peaks not belonging to the M1 and M2 phases are marked as follows: $Al_2(MoO_4)_3$ (∗), $AlVO_4$ (▼), $TeMo_5O_{16}$ (■), Nb_2O_5 (▲), and TiO_2 (□).

Table 2
Phases present in the prepared samples as determined by XRD

Sample	Crystalline phases observed by XRD
X1	M1
X1AS	$Al_2(MoO_4)_3$, $AlVO_4$, $TeMo_5O_{16}$, Nb_2O_5
X1SS	M1
X1TS	TiO_2 (anatase), $Mo_{5-x}(V/Nb)_xO_{14}$, Nb_2O_5
X2	M2
X2AS	M2, $Al_2(MoO_4)_3$
X2SS	M2
X2TS	M2, TiO_2 (anatase)
X3	M1, M2
X3AS	$Al_2(MoO_4)_3$, $AlVO_4$, $TeMo_5O_{16}$, Nb_2O_5
X3SS	M1, M2
X3TS	M1, M2, TiO_2 (anatase)

3.2. Temperature-programmed reduction

The TPR profiles of the neat and sol-diluted samples are given in Figs. 4–6. TPR was performed because it is sensitive to the phase composition, in that under specified conditions, each phase gives a characteristic reduction profile, containing information about the reduction sequence/pathway over one or several intermediate and reduced phases. Shifts in peak positions, relative to a reference sample of the same phase, gives qualitative information about the particle size. Moreover, in the case of mixed-oxide samples, peak shifts may reveal interaction between the phases. With these aspects in mind, the TPR profiles of the catalysts in Figs. 4–6 are presented and discussed in relation to the corresponding XRD data.

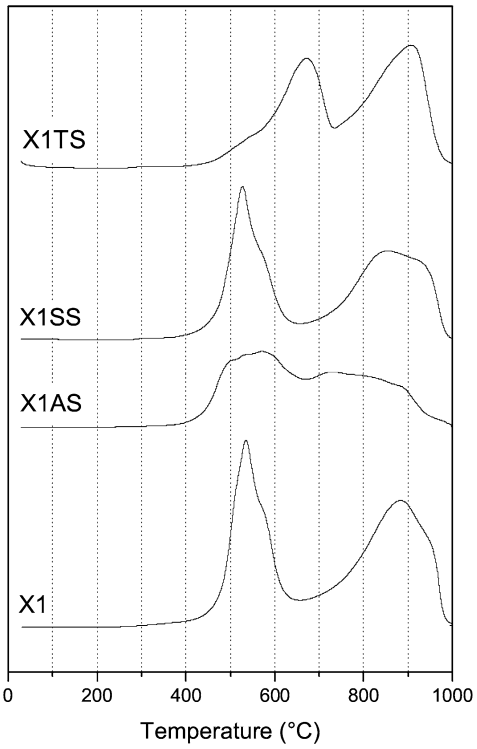

Fig. 4. Weight-normalised TPR profiles of the X1, X1AS, X1SS, and X1TS catalysts.

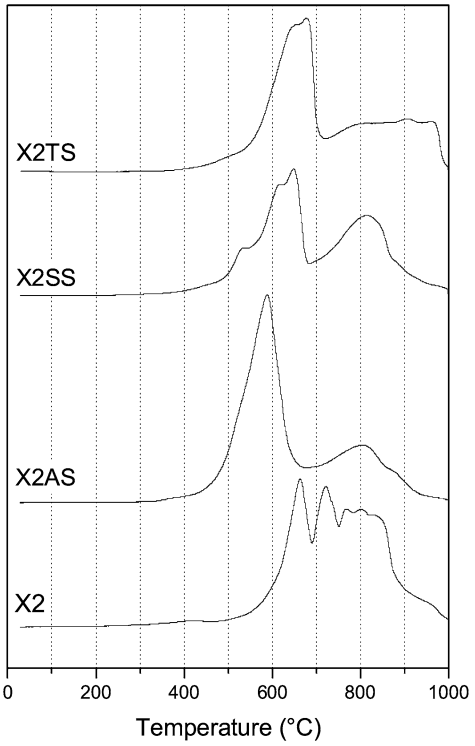

Fig. 5. Weight-normalised TPR profiles of the X2, X2AS, X2SS, and X2TS catalysts.

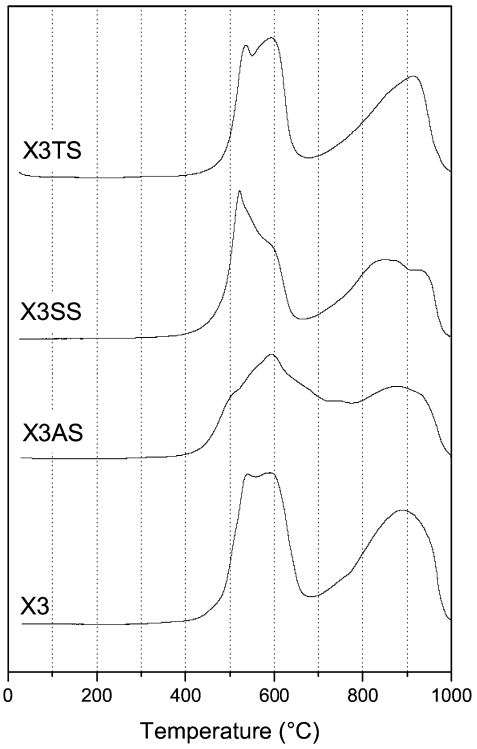

Fig. 6. Weight-normalised TPR profiles of the X3, X3AS, X3SS, and X3TS catalysts.

Considering the TPR profiles in Fig. 4 for the neat and diluted X1 catalysts, the TPR profile of the X1 sample shows two doublet peaks with maxima at 534/574 °C and 887/960 °C, respectively. X1SS gives a very similar reduction profile, in agreement with XRD (Fig. 1), demonstrating that both samples contain the M1 phase. However, compared with the TPR profile for the neat X1 sample, the peak maxima in the profile of X1SS are shifted toward somewhat lower temperatures, namely 523/563 °C and 850/940 °C, respectively. These shifts suggest that the M1 crystallites are smaller in X1SS than in X1, an indication supported by the XRD patterns in Fig. 1 showing broader M1 peaks for X1SS ($FWHM_{(002)} = 0.106°$) than for X1 ($FWHM_{(002)} = 0.101°$). The TPR pattern for X1TS with $Mo_{5-x}(V/Nb/Te)_xO_{14}$ has some similarities with the profiles for X1 and X1SS, although the first major reduction maxima at 676 °C appears to be compared with that at ∼530 °C for X1 and X1SS. The similar reduction profiles are due to M1 and $Mo_{5-x}(V/Nb/Te)_xO_{14}$ having similar structural elements in that both compounds have pentagonal bipyramidal metal sites sharing edges in (110) with five octahedral sites [7,19]. Compared with X1, X1SS, and X1TS, the X1AS sample gives a broader TPR profile with several small maxima. These features are in line with X1AS consists of several phases, as shown in Table 2.

The reduction profiles in Fig. 5 for the X2 compositions reveal clear differences between the samples despite the fact that all contain the M2 phase (Table 2). X2SS and X2TS show similar reduction profiles in the range of 400–700 °C, where the former sample shows three peaks (532, 614, and 651 °C), whereas a shoulder (500 °C) and two peaks (651 and 677 °C) are resolved for the latter. The fact that the two peaks between 600 and 700 °C are at about a 30 °C lower temperature for X2SS than for X2TS indicates that on average, the M2 crystallites are smaller in the former sample (see below). Moreover, it is noticeable that above 700 °C, X2SS shows a well-developed reduction peak at 813 °C, whereas X2TS gives a broad reduction feature extending from ∼750 to 970 °C. The broad feature may be caused by interaction between the M2 phase and the TiO_2. Support for such interaction is the finding that Ti can be incorporated into the M2 structure [16], which may affect the reduction not only at above 700 °C, but also at lower temperatures. Remarkable is that the neat X2 sample has a reduction profile very different from those shown by X2SS and X2TS, despite the fact that all contain M2. The discrepancy may be due to the M2 in X2, compared with the M2 in X2SS and X2TS, either having different distributions of surface planes or consisting of larger particles, the reduction of which requires higher temperatures. Examining the XRD peaks in Fig. 2 shows that the peaks for the X2 sample are narrower ($FWHM_{(630)} = 0.079°$) than the corresponding peaks for X2SS ($FWHM_{(630)} = 0.094°$) and X2TS ($FWHM_{(630)} = 0.085°$), demonstrating that the M2 crystallites are larger in X2 than in the latter two samples. The reduction profile for the X2AS sample shows one large peak at 589 °C and smaller peaks above 700 °C. According to XRD (Table 2), the sample consists of M2 and $Al_2(MoO_4)_3$. However, the intensities of the XRD peaks are relatively low. Thus, it seems that the sample may contain some XRD amorphous material as well, explaining the fact that the reduction is smooth and continuous, producing one peak only. Of course, interaction between the constituent phases and their reduction products also may affect the reduction behavior.

The TPR profiles of the X3 compositions are given in Fig. 6, which shows similar reduction profiles for X3, X3SS, and X3TS. This observation is not surprising in view of the fact that they all contain the M1 and M2 phases (Table 2). The minor differences between the reduction profiles of these samples can be due to some differences in their distribution of particle sizes and phase ratios. Both X3 and X3SS are reduced at 500–600 °C, in agreement with the corresponding samples with M1 (X1 and X1SS in Fig. 4), whereas the corresponding samples with M2 (X2 and X2SS in Fig. 5) are reduced at about 100 °C higher. In addition, X3TS is reduced at lower temperatures than X2TS. These observations indicate that there is some type of interaction between the constituent M1 and M2 phases, or their reduction products influencing the progress of the reduction process. The TPR profile for X3AS shows resemblance to that for X1AS, in agreement with both samples contain the same crystalline phases (Figs. 1 and 3).

3.3. Catalytic performance

The neat and the diluted X1 and X3 catalysts were used for propane ammoxidation, and the corresponding X1 and X2 catalysts were used for propene ammoxidation. The choice was made considering that of the M1 and M2 phases, only the M1 phase is active for propane ammoxidation and oxidation, whereas M2 is inactive [13,15,21]. Moreover, both M1 and

M2 are active for ammoxidation of propene, a reaction for which the M2 phase has been reported to be more selective than M1 [13]. Consequently, the best propane ammoxidation catalyst should contain both M1 and M2 in a proper ratio and intimately mixed, allowing the propene formed from propane on M1 to readsorb on M2, forming acrylonitrile [13]. In the present study, it was confirmed that the samples X2, X2AS, X2SS, and X2TS, containing M2 but no M1, all showed practically no activity for propane ammoxidation.

3.3.1. Ammoxidation of propene and propane on the X1 compositions

The catalytic data in Fig. 7 for propene ammoxidation on the neat and the diluted X1 catalysts show that X1 and X1SS are the two most active catalysts, whereas X1TS and especially X1AS present considerably lower activity. According to the recorded XRD patterns (Fig. 1), only the two most active catalysts contain the M1 phase. Table 3 presents a comparison of the activities calculated per surface area unit of catalyst and per mass unit of active metals, respectively. The data in the table shows that X1SS is more active than the neat X1 per mass unit of active metals, in agreement with the XRD and TPR results (Figs. 1 and 4), indicating better dispersion, that is, smaller M1 crystallites in X1SS (see Section 3.2). Moreover, the selectivity data in Fig. 7 show that X1SS is somewhat more selective than X1 for acrylonitrile formation, with selectivities of 58% and 51%, respectively, at 70% propene conversion. The low activity of X1TS and X1AS can be related to the absence of M1 in these samples (Table 2). Despite their low activity, it is interesting that both samples are selective to acrylonitrile with selectivity values similar to those for X1 and X1SS.

Compared with propene ammoxidation, the X1 compositions are considerably less active for propane ammoxidation, as the data in Fig. 8 and Table 3 show. Here the activity of the neat X1 is fourfold lower, and that of X1AS and X1TS is tenfold lower, than in propene ammoxidation. These data, of course, are in agreement with the activation of propane being considerably more difficult than that of propene. More surprising, however, is that despite the fact that X1SS per mass unit of active metals is more active than X1 for propene ammoxidation, which agrees with the observed difference in crystallite size (see above), it is the reverse in propane ammoxidation. This result clearly indicates that despite the fact that both samples contain M1 (Table 2), there is some difference in their surface structure, for example, surface roughness. The difference is also confirmed by the selectivity variation with propane conversion, as Fig. 8 shows. On X1, the selectivity to acrylonitrile increases with increase of the conversion, whereas on X1SS, it virtually does not vary. Another difference is that more of the formed propene is consecutively transformed to acrylonitrile on X1 than on X1SS. The latter sample seems to burn

Table 3
Comparison of the activities of the neat and the sol-diluted X1, X2, and X3 samples

Catalyst	Propene ammoxidation		Propane ammoxidation	
	μmol/(m^2 min)	μmol/(g AM min)[a]	μmol/(m^2 min)	μmol/(g AM min)
X1	68.5	415.1	16.8	101.6
X1AS	1.9	46.4	0.2	3.8
X1SS	57.5	713.9	2.3	28.0
X1TS	20.7	37.3	1.9	3.4
X2	5.0	12.6	ND[b]	ND
X2AS	2.5	27.0	ND	ND
X2SS	2.2	20.1	ND	ND
X2TS	12.2	82.4	ND	ND
X3	ND	ND	8.0	41.7
X3AS	ND	ND	0.1	1.6
X3SS	ND	ND	2.8	31.0
X3TS	ND	ND	4.4	15.2

[a] AM: active metals (Mo, V, Te and Nb).
[b] ND: not determined.

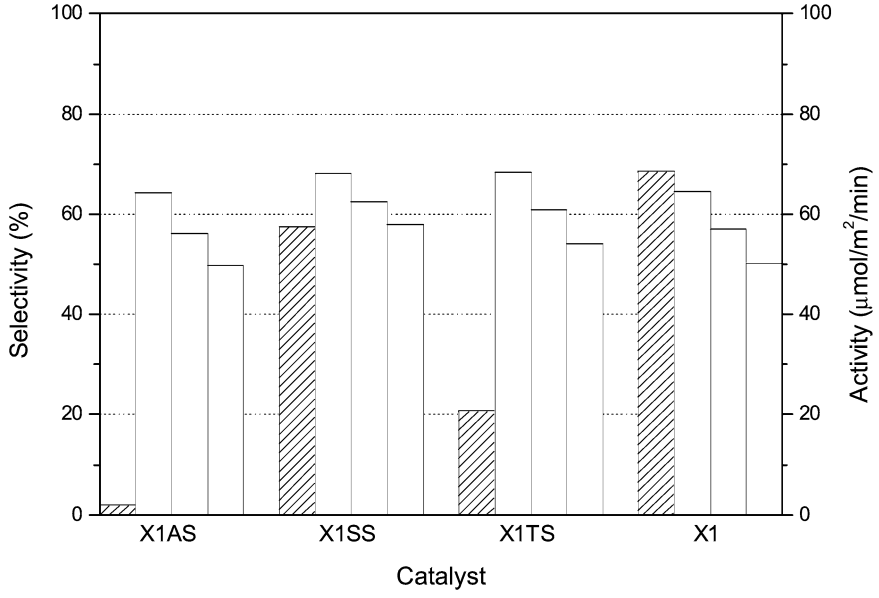

Fig. 7. Ammoxidation of propene on the neat X1 catalyst and the corresponding sol-diluted catalysts. The bars from left to right represent the activity (▨) and the selectivity to acrylonitrile (□) at 20, 50, and 70% propene conversion, respectively. For experimental conditions, see Section 2.2.

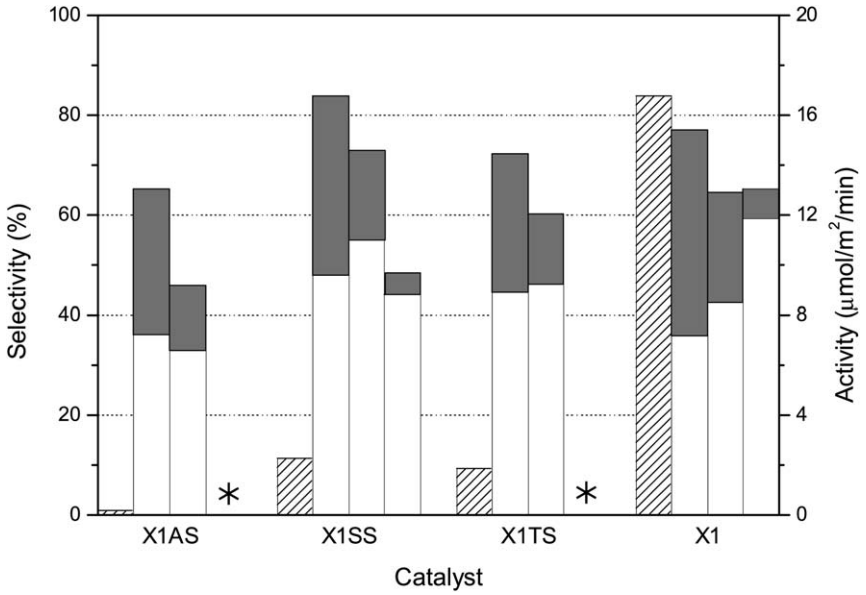

Fig. 8. Ammoxidation of propane on the neat X1 catalyst and the corresponding sol-diluted catalysts. The bars from left to right represent the activity (▨) and the selectivity to acrylonitrile (□) and propene (■) at 10, 20, and 50% propane conversion, respectively. Due to experimental limitations, data is missing (∗) for X1AS and X1TS at 50% propane conversion. For experimental conditions, see Section 2.2.

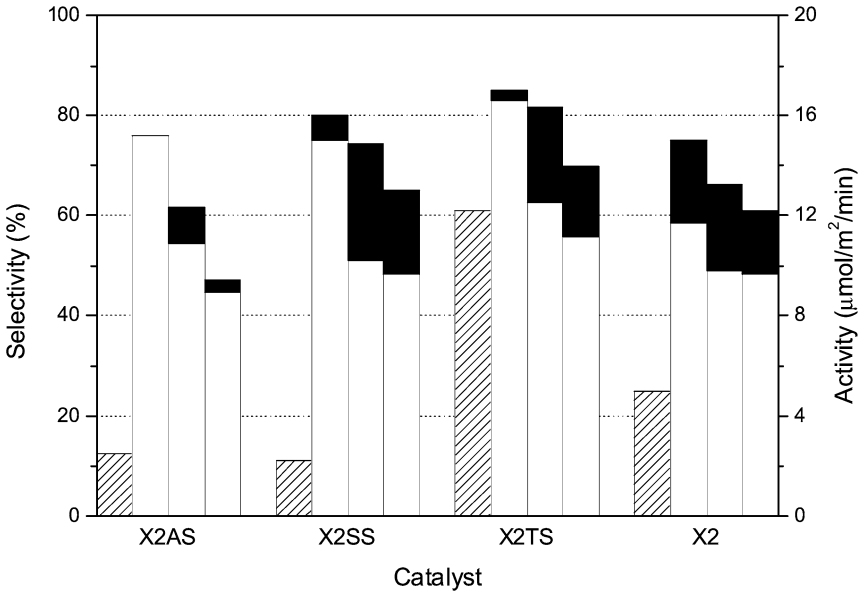

Fig. 9. Ammoxidation of propene on the neat X2 catalyst the corresponding sol-diluted catalysts. The bars from left to right represent the activity (▨) and the selectivity to acrylonitrile (□) and acrolein (■) at 20, 50, and 70% propene conversion, respectively. For experimental conditions, see Section 2.2.

a large part of the propene, which is not due to lack of ammonia, as evidenced by the fact that the yield of acrylonitrile (conversion × selectivity/100) is steadily increasing from 10 to 50% propane conversion.

Although X1TS and X1AS do not contain M1 (Table 2) and have low activity for propane ammoxidation, especially per mass unit of active metals, the samples give both propene and acrylonitrile as products. However, the selectivity to propene decreases with increasing propane conversion, and the selectivity to acrylonitrile remains rather constant.

Of the X1 compositions, considering both activity and selectivity data for propane ammoxidation, the neat X1 is the most active and best-performing catalyst followed by X1SS. The data in Fig. 8 show that at 50% propane conversion, X1 and X1SS give selectivities to acrylonitrile of 59 and 45%, respectively, together with ∼3–5% of propene. At lower conversions, X1SS is more selective than X1.

3.3.2. *Ammoxidation of propene on the X2 compositions*

Activity and selectivity data are shown in Fig. 9 and Table 3 for propene ammoxidation on the X2-type of catalysts with the M2 phase (Fig. 2). Notable is that the titania-diluted sample X2TS is the most active catalyst. Comparing the activities per mass unit of active metals (Table 3), it is apparent

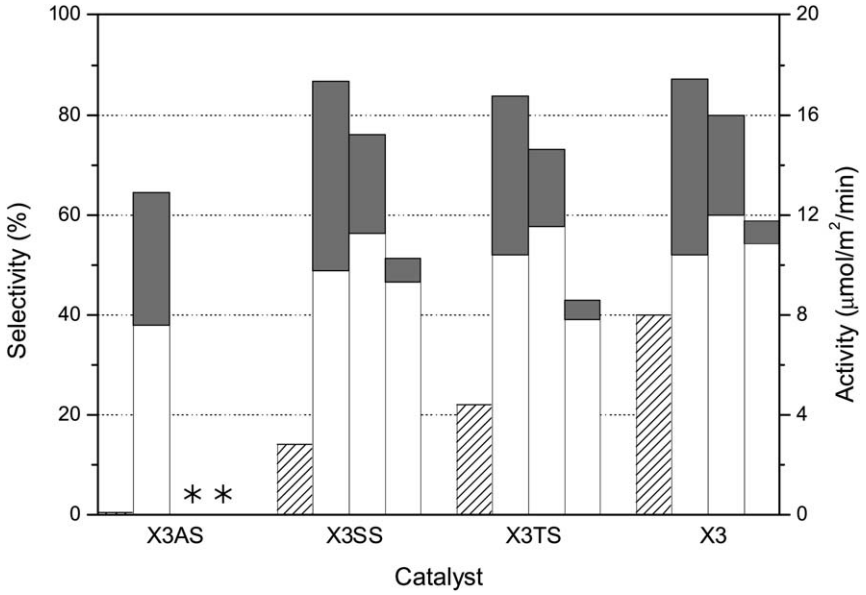

Fig. 10. Ammoxidation of propane on the neat X3 catalyst and the corresponding sol-diluted catalysts. The bars from left to right represent the activity (▨) and the selectivity to acrylonitrile (□) and propene (■) at 10, 20, and 50% propane conversion, respectively. Due to experimental limitation, data is missing (∗) for X3AS at 20 and 50% propane conversion. For experimental conditions, see Section 2.2.

that all of the diluted samples are more active than the neat X2. Compared with the activity for X2, the activities for X2AS and X2SS are about twofold higher, and the activity for X2TS is more than sixfold higher. The increased activity per mass unit of active metal, achieved by dilution of the M2 phase, is due to dilution resulting in formation of smaller M2 crystallites, as evidenced by the peak broadening seen on XRD and the TPR results (see Section 3.2). The fact that the activity is significantly higher for X2TS than for the other diluted samples is in agreement with our earlier investigation [16], showing that partial substitution of Ti^{4+} for V^{4+} in M2 is possible and leads to considerable increase in the activity. It was proposed that the increase is achieved through adjustment of the Mo–O distances of the active Mo site.

In agreement with all samples contain the M2 phase, Fig. 9 shows that the selectivities to the formations of acrolein and acrylonitrile are similar in the different samples, except for X2AS, with some $Al_2(MoO_4)_3$ giving less acrolein. Concerning the selectivity to acrylonitrile specifically, X2TS is the most selective sample with selectivities of 83 and 55% at 20 and 70% propene conversions, respectively. Opposed to the X1 preparations (Fig. 7), the X2 samples also produce acrolein, resulting in a higher total selectivity to C_3 products. Moreover, the neat X2 with the pure M2 phase is considerably less active than the neat X1 sample with pure M1 phase. This finding is opposed to our previous results, indicating that M1 and M2 have similar activities for propene ammoxidation [12]. The most likely explanation for this discrepancy is that the present synthesis of M1 (X1) was made using flash drying at 200 °C, whereas in the previous investigations [12,13], slower evaporation was performed at lower temperatures. It is well known that the performance of M1 depends strongly on the details of the synthesis [22–25].

3.3.3. Ammoxidation of propane on the X3 compositions

The propane ammoxidation data in Fig. 10 and Table 3 for the X3 compositions show that X3, X3TS, and X3SS are considerably more active than X3AS. Opposed to the latter sample, the former three samples contain the M1 and M2 phases (Fig. 3), and their activity per mass unit of active metals decreases in the order X3 > X3SS > X3TS (Table 3). The activity trend suggests that either the crystallite sizes of the active material or the number of propane activating sites per mass unit of active metals should decrease in the same order. The latter explanation is the most likely, considering that the TPR profiles in Fig. 6 do not support any difference in particle size, because they show approximately the same reduction temperature for the samples. However, there are differences in the fine details of the profiles, which in this case are difficult to relate directly to the catalytic performance, because the samples contain two reducible phases, M1 and M2.

As expected, compared with the neat X1 sample, the neat X3 sample is less active for propane ammoxidation (Table 3), which is consistent with only the M1 phase being active for propane ammoxidation [13,15]. In contrast, X3TS containing M1 and M2 is more active than X1TS, which can be explained by the fact that the latter sample is without the M1 phase (Table 2). The X3AS and X1AS samples have low but rather similar activity and also have similar selectivity to acrylonitrile and propene, which is consistent with the fact that both samples consist largely of the same phases but neither M1 nor M2. More striking, however, is that X3SS with both M1 and M2 has the same activity as X1SS with M1 only. This result clearly indicates good dispersion of the M1 phase in X3SS, which is also consistent with the fact that the TPR profile for X3SS in Fig. 6 shows great similarity to those in Fig. 4 for the M1-containing samples X1 and X1SS. Moreover, the selectivities to propene and acrylonitrile obtained over X3SS at

different propane conversions (Fig. 10) largely agree with the corresponding values measured for X1SS (Fig. 8). Thus, the performance of X3SS is determined by the M1 phase, agreeing with the fact that the M1-containing catalysts X1 and X1SS are active for propane and more active than the M2-containing X2 and X2SS catalysts for propene ammoxidation. In contrast, the X3TS sample is more selective than the X1TS sample, due mainly to the fact that X3TS contains M1 and M2, whereas X1TS contains $Mo_{5-x}(V/Nb/Te)_xO_{14}$. The fact that the neat X3 catalyst shows higher selectivity to acrylonitrile at low propane conversion compared with the neat X1 indicates some contribution from the M2 phase in this case.

In terms of both activity and selectivity, the best-performing X3 compositions are the neat X3, followed by X3SS and X3TS. At 10 and 20% conversion levels, the selectivities to propene and acrylonitrile, and their variation with the conversion of propane, are rather similar for these samples. However, at a 50% conversion level, the differences between the catalysts are more evident. Here the selectivity to acrylonitrile is the highest for X3, 54% compared with 46% for X3SS and 38% for X3TS. The differences in performance are consistent with XRD (Fig. 3) and TPR (Fig. 6) results showing some differences between the samples. A comparison of the XRD patterns in Fig. 3 reveals that the M2/M1 ratio decreases in the order X3 > X3SS > X3TS, suggesting that there might be an optimal ratio for propane ammoxidation.

4. Conclusion

Of the SiO_2, TiO_2, and Al_2O_3 sols used as additives (dilutants, binders), SiO_2 is the most inert material with respect to the formations of M1 and M2. Dilution of the M1 composition with TiO_2 gives $Mo_{5-x}(V/Nb/Te)_xO_{14}$ and not M1. However, the corresponding syntheses with the M2 and M1/M2 compositions give the correct phase and phase mixture. Alumina is the least inert of the additives because it reacts with Mo and V, resulting in the formation of $Al_2(MoO_4)_3$, $AlVO_4$, $TeMo_5O_{16}$, and Nb_2O_5.

For propane ammoxidation, considering both the activity per unit surface area of catalyst and the selectivity to acrylonitrile plus propene, the neat M1 and M1/M2 catalysts are the best catalysts. At 50% propane conversion, they give a total selectivity of 65 and 59%, respectively, of which ∼5% is propene. The second-best catalysts are the corresponding compositions diluted with SiO_2 with a total selectivity of about 50%, including 4% to propene.

For propene ammoxidation, the SiO_2-diluted M1 and the neat M1 are the best catalysts based on M1 with selectivities to acrylonitrile of 58 and 51%, respectively, at 70% propene conversion. These samples do not produce acrolein, which is the case for catalysts with M2 only. In addition, the M2 catalysts are less active than the corresponding M1 catalysts. Of the M2 catalysts, the preparation diluted with TiO_2 is the most active and selective catalyst, with selectivities to acrylonitrile and acrolein of 55 and 14%, respectively, at 70% propene conversion. It has been shown previously that the acrolein formed on M2 can be converted completely to acrylonitrile by increasing the propene:ammonia ratio from 1 to 2 [13]. Another alternative is to substitute some W for Mo, which has been reported to increase the selectivity to acrylonitrile on behalf of the selectivity to acrolein [16].

One purpose of the present investigation was to use sol dilution to increase the dispersion of the M1 and M2 phases. Compared with the neat M1 and M2 samples, XRD and TPR show that dilution with silica gives somewhat smaller M1 crystallites, and dilution with silica or titania give smaller M2 crystallites. However, the increased dispersion is not sufficient to compensate for the dilution, as evidenced by the fact that in most cases there is no corresponding increase in the activity expressed per surface area unit of the catalyst.

Concerning the interplay between M1 and M2 in propane ammoxidation, the activity and selectivity data for the M1/M2 catalysts do not indicate much improvement due to dilution. A reason for this might be the fact that the symbiosis between the phases is not optimized with regard to particle size, mixing of the phases, and their ratio. Compared with the neat M1/M2, according to XRD, dilution with SiO_2 and TiO_2 give higher M1/M2 ratios.

Despite the fact that dilution does not give the desired dispersion effect, dilution of the active M1 and M2 compositions remains of interest for fluid-bed applications to increase the catalyst's attrition resistance.

Acknowledgments

Financial support from the Swedish Research Council is acknowledged.

References

[1] R.K. Grasselli, in: G. Ertl, H. Knözinger, J. Weitkamp (Eds.), Handbook of Heterogeneous Catalysis, Wiley/VHC, New York, 1997, pp. 2302–2326.
[2] L. Kihlborg, Acta Chem. Scand. 13 (1959) 954.
[3] L. Kihlborg, Arkiv Kemi 21 (1963) 427.
[4] T. Ushikubo, K. Oshima, A. Kayo, T. Umezawa, K. Kiyono, I. Sawaki, European Patent 529 853 (1992), to the Mitsubishi Chemical Corporation, Tokyo, Japan.
[5] S. Komada, H. Hinago, M. Kaneta, M. Watanabe, European Patent 895 809 (1998), to Asahi Kasei Kogyo Kabushiki Kaisha, Osaka, Japan.
[6] T. Ushikubo, K. Oshima, A. Kayou, M. Hatano, in: C. Li, Q. Xin (Eds.), Spillover and Migration of Surface Species on Catalysts, Stud. Surf. Sci. Catal., vol. 112, Elsevier, Amsterdam, 1997, pp. 473–480.
[7] P. DeSanto Jr., D.J. Buttrey, R.K. Grasselli, C.G. Lugmair, A.F. Volpe Jr., B.H. Toby, T. Vogt, Z. Kristallogr. 219 (2004) 152.
[8] J.M.M. Millet, H. Roussel, A. Pigamo, J.L. Dubois, J.C. Jumas, Appl. Catal. A 232 (2002) 77.
[9] M. Baca, J.-M.M. Millet, Appl. Catal. A 279 (2005) 67; Erratum: Appl. Catal. 288 (2005) 243.
[10] M. Lundberg, M. Sundberg, Ultramicroscopy 52 (1993) 429.
[11] A. Magnéli, Acta Chem. Scand. 7 (1953) 315.
[12] J. Holmberg, R.K. Grasselli, A. Andersson, Top. Catal. 23 (2003) 55.
[13] J. Holmberg, R.K. Grasselli, A. Andersson, Appl. Catal. A 270 (2004) 121.
[14] P. DeSanto Jr., D.J. Buttrey, R.K. Grasselli, C.G. Lugmair, A.F. Volpe Jr., B.H. Toby, T. Vogt, Top. Catal. 23 (2003) 23.
[15] R.K. Grasselli, J.D. Burrington, D.J. Buttrey, P. DeSanto Jr., C.G. Lugmair, A.F. Volpe Jr., T. Weingand, Top. Catal. 23 (2003) 5.
[16] J. Holmberg, S. Hansen, R.K. Grasselli, A. Andersson, Top. Catal. 38 (2006) 17.

[17] JCPDS International Centre for Diffraction Data, Powder Diffraction File, Swarthmore, PA (1991).
[18] W.T.A. Harrison, A.K. Cheetham, J. Faber Jr., J. Solid State Chem. 76 (1988) 328.
[19] P. Botella, E. García-González, A. Dejoz, J.M. López Nieto, M.I. Vázquez, J. González-Calbet, J. Catal. 225 (2004) 428.
[20] R.D. Shannon, Acta Crystallogr. Sect. A 32 (1976) 751.
[21] P. Botella, J.M. López Nieto, B. Solsona, Catal. Lett. 78 (2002) 383.
[22] J.M. López Nieto, P. Botella, B. Solsona, J.M. Oliver, Catal. Today 81 (2003) 87.
[23] J.M. Oliver, J.M. López Nieto, P. Botella, A. Mifsud, Appl. Catal. A 257 (2004) 67.
[24] M.M. Lin, Appl. Catal. A 250 (2003) 287.
[25] M.M. Lin, Appl. Catal. A 250 (2003) 305.